THE ASTROPHYSICAL JOURNAL, 278:791–805, 1984 March 15

VORTEX CREEP AND THE INTERNAL TEMPERATURE OF NEUTRON STARS. II. VELA PULSAR[1]

M. A. ALPAR
Physics Department, Bogazici University, Istanbul; and
Physics Department, University of Illinois at Urbana-Champaign

P. W. ANDERSON
Bell Laboratories, Murray Hill, New Jersey; and
Department of Physics, Princeton University

D. PINES
Physics Department, University of Illinois at Urbana-Champaign

AND

J. SHAHAM
Racah Institute of Physics, Hebrew University, Jerusalem, Israel; and
Physics Department, Columbia University
Received 1983 May 13; accepted 1983 August 22

ABSTRACT

The observed complex postglitch behavior of the Vela pulsar is explained as resulting from coupling of the crust to crustal neutron superfluid, specifically that part of the superfluid in which vortex lines are pinned to crustal nuclei. We show how the general theory of vortex creep developed in a preceding paper provides an excellent fit to the timing observations of Downs which span the decade 1969–1979 and include four giant glitches. We extract from our fit to the data relaxation times, inertial moments, and limits on superfluid pinning parameters for three distinct regions of vortex pinning in the star, with results which are consistent with microscopic theories of its internal structure. In our theory, relaxation times due to vortex creep are directly proportional to the internal temperature of the star, so that the limits we obtain for pinning parameters translate to bounds on this temperature. We conclude that the internal temperature of the Vela pulsar is $\sim 10^7$ K and discuss the extent to which improved calculations of vortex pinning as well as soft X-ray observations of other stars will make possible an improved determination of the pulsar temperature.

Subject headings: dense matter — pulsars — stars: neutron

I. INTRODUCTION

In the first paper in this series (Alpar *et al.* 1984, hereafter Paper I) we developed a general theory of vortex creep, the motion of vortex lines in that portion of the neutron superfluid which permeates the crust of a neutron star and is pinned to the crustal nuclei. We showed that for many physically plausible situations, a simple set of equations suffices to describe the coupling of the pinned superfluid to the crust. We further suggested that vortex creep is likely to be the dominant mechanism by which the pinned crustal neutron superfluid keeps pace with the crust as a neutron star is spun up or down by an external torque, and found that the relaxation times which characterize this coupling offer promise of being observable in the behavior of those stars which exhibit glitches. These relaxation times are proportional to the internal temperature of the neutron star, so that studies of postglitch behavior offer the considerable promise of providing a measure of the temperature.

The Vela pulsar has exhibited both more frequent and "larger" giant glitches than any other pulsar. Moreover, Downs (1981) has recently published the results of a monumental series of timing observations which span more than a decade and include four giant glitches. It is therefore a natural candidate for a first application of our theory of vortex creep. In § II, following a brief review of the observational results, we show how the theory developed in Paper I provides an excellent fit to the observed complex postglitch behavior of the pulsar. A glitch acts to stop vortex creep and thus to decouple temporarily from the crust all regions of pinned vorticity in the star. We conclude from our fit to the data that internal torques from at least three such regions contribute to postglitch behavior. Two of these torques correspond to the time-dependent recoupling of physically distinct regions in which glitch-induced vortex motion does not take place; the relaxation times which characterize vortex creep in these regions are $\sim 3^d$ and 60^d, respectively. The third torque, which varies linearly with time, is produced by the gradual recoupling of vortex creep in the boundary between the above regions, a recoupling which is determined by the glitch-induced vortex motion which occurs there. In § III we use a simple model of glitch-induced vortex motion to place limits on the parameters which determine this torque. In § IV we extract from our fit to the data inertial moments and limits on superfluid pinning parameters for the two regions in which glitch-induced vortex motion has not occurred, and show that our results are consistent with microscopic

[1] This research was supported in part by NSF grants PHY 80-25605, PHY 80-23721, NASA grants NAS8-3073, US NASA NSG-7653, and NATO Research Grant RG 186-81.

TABLE 1

OBSERVED PARAMETERS FOR THE FIRST FOUR VELA GLITCHES

Quantity	Glitch 1	Glitch 2	Glitch 3	Glitch 4
$\Delta\Omega_c$ (10^{-4} rad s^{-1})	1.65	1.39	1.42	2.16
$\Delta\dot{\Omega}_c/\dot{\Omega}_c \equiv \bar{I}_p/I$ (10^{-2})	0.93	1.49	1.00	2.58
$\delta\bar{\Omega}_p \equiv \Delta\Omega_c/(\bar{I}_p/I)$ (10^{-2} rad s^{-1})	1.77	0.93	1.42	0.84
Δ_m (days)	7	14	5	23
$t_0 \equiv \Delta\Omega_c/\lvert\dot{\Omega}_c\rvert$ (days)	19	16	16.5	25

NOTE. —$\Delta\Omega_c$ is the jump in observed rotation frequency, $\Delta\dot{\Omega}_c/\dot{\Omega}_c$ the fractional jump in spindown rate, and Δ_m the time between the last preglitch observations and the first postglitch observations.

theories of neutron star superfluidity and structure. We use these results in § V to estimate the internal temperature of the Vela pulsar, and in this way obtain temperature limits which are sensitive mainly to the (in principle) calculable distance between pinning sites. We consider as well information on vortex pinning and energy dissipation in neutron stars which may be obtained from soft X-ray observations such as those carried out by Helfand (1982) using the *Einstein* observatory. We discuss our results in § VI.

II. POSTGLITCH BEHAVIOR

Before making a comparison of the theory we presented in Paper I with observation for the Vela pulsar, we review briefly the overall observational situation. Thus far six glitches have been observed (Radhakrishnan and Manchester 1969; Reichley and Downs 1969, 1971; Manchester, Goss, and Hamilton 1976; Downs, Manchester, and Newton 1978; McCulloch, Hamilton, and Royle 1981; Hamilton, McCulloch, and Royle 1982; McCulloch *et al.* 1983). We apply our theory to the detailed postglitch observations for the first four glitches (Downs 1981). A general overview of these glitches is presented in Table 1. The timing behavior following glitch 5 published recently by McCulloch *et al.* (1983) appears similar to that found in the earlier glitches.

One can define, as we did in earlier work (Alpar *et al.* 1981), an effective moment of inertia $\bar{I}_p$ of the neutron superfluid in the pinning layers of the star from the observed jump in the time derivative of the crustal frequency, $\Delta\dot{\Omega}_c$, which is found to accompany each glitch:

$$\bar{I}_p/I \equiv \Delta\dot{\Omega}_c/\dot{\Omega}_c \,. \tag{1}$$

Here Ω_c and $\dot{\Omega}_c$ are the observed rotation and spin-down rates of the pulsar crust and I denotes the total moment of inertia of the star. We define a mean decrease $\delta\bar{\Omega}_p$ in the superfluid rotation rate in these layers as found from:

$$\bar{I}_p\,\delta\bar{\Omega}_p = I_c\,\Delta\Omega_c \,, \tag{2}$$

where $\Delta\Omega_c$ is the glitch in Ω_c. The moment of inertia I_c represents the crust and all components of the star that are coupled to it on time scales $\lesssim$hours. Recent calculations show that the superfluid in the core of the neutron star couples to the crust with coupling times of the order of seconds (Alpar, Langer, and Sauls 1984). Thus I_c includes the entire star except the pinned superfluid. In Table 1 we have listed the observed values for $\Delta\Omega_c$ and the postglitch delay time t_0, which we defined in equation (45) of Paper I, (I.45),

$$t_0 = \frac{\Delta\Omega_c}{\lvert\dot{\Omega}\rvert_\infty} \approx \left(\frac{\Delta\Omega_c}{\Omega_c}\right) t_s \tag{3}$$

where $\dot{\Omega}_\infty = N/I$ is the steady state spin-down rate (cf. eq. [I.20]) of the Vela pulsar, which in the applications that follow can be taken to be given by

$$\lvert\dot{\Omega}\rvert_\infty \equiv \Omega_c/t_s \approx 9.83 \times 10^{-11} \text{ rad s}^{-2}$$

on taking t_s, the pulsar spindown time, as 2.27×10^4 yr. We also tabulate the uncertainty, Δ_m, in the actual time at which the glitch took place.

The general features of post-glitch behavior are best appreciated by examining the behavior of $\dot{\Omega}_c$, since it is here that the influence of the internal torque produced by the coupling of the neutron superfluid to the crust is most clearly manifested. As may be seen in Figures 1*a*–1*h*, the postglitch behavior of the Vela pulsar after each of the first four glitches is rather complex, in that it is clearly not describable by a single exponential relaxation process, and would seem to be a superposition of several different internal torques. More specifically, we find the following characteristic behavior after each of the first four glitches:

1. Within the first 20 days or so after the glitch, there is comparatively rapid relaxation of one component, whose contribution to the internal torque we denote by N_1.
2. A second component of the internal torque, N_2, relaxes with a characteristic time $40^d \lesssim \tau \lesssim 100^d$.
3. A third component, N_A, varies linearly with time, and is thus responsible for the $\ddot{\Omega}_c \approx$ constant behavior observed by Downs.
4. As is the case for $\Delta\Omega_c$, $\bar{I}_p$, and $\delta\bar{\Omega}_p$, each of the internal torques varies somewhat from glitch to glitch; however, their general order of magnitude remains the same.

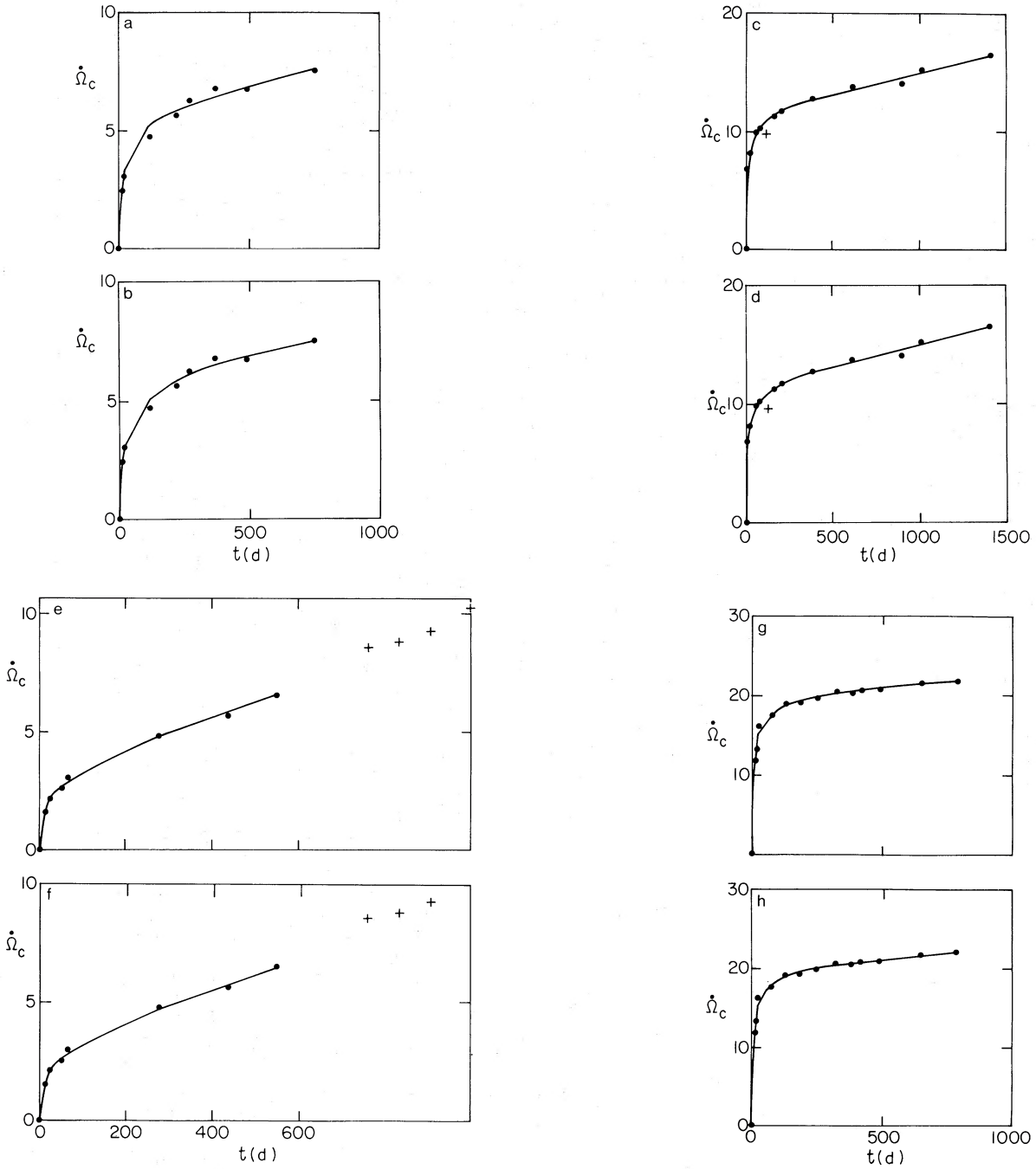

FIG. 1.—Fits to the postglitch $\dot{\Omega}_c(t)$ in each of the first four Vela glitches. The figures refer to the glitches in chronological order. For each glitch the first figure (1*a*, 1*c*, 1*e*, 1*g*) shows the fit with $\tau_1 = 3^d$, $\tau_2 = 60^d$. The second figure in each pair (1*b*, 1*d*, 1*f*, 1*h*) shows the best fit. Data points are $\dot{\Omega}_c(t) - \dot{\Omega}_c(0)$ from Downs's $\dot{P}$ observations (Downs 1981) in units of 10^{-15} rad s^{-2}. The time $t = 0$ is the time of the first postglitch data point; t is given in days. The crosses in Figs. 1*c*, 1*d* (postglitch 2) and 1*e*, 1*f* (postglitch 3) are data points not included in the fit. They are discussed in the text. The fitting function is given in eq. (9).

As we have emphasized in Paper I, a glitch leads to the temporary decoupling of *all* regions of pinned vorticity in the crust; we interpret the postglitch behavior as reflecting the recoupling of the neutron superfluid by vortex creep in these various regions. Microscopic calculations strongly suggest substantial variations in the pinning parameters which determine vortex creep as one goes through the pinning region. We therefore expect this recoupling to give rise to distinct torques representing regions characterized by distinct rates of vortex creep. We have also seen in Paper I that the postglitch vortex creep of a given region depends sensitively on the influence of the glitch on that region. More specifically, *in those regions of the star through which no vortices travel in the course of a glitch, the changed rate of thermal creep represents a response solely to* $\Delta\Omega_c$; it is characterized by a relaxation time τ and the postglitch delay time t_0, equation (3). It is natural to represent the response of these regions by at least

two distinct internal torques, since we expect the glitch to take place in a boundary region, on either side of which the relaxation times, τ_i, may be expected to be different. These are from equation (I.44):

$$\frac{N_i(t)}{|N|} = \frac{I_i}{I} \frac{1}{1 + [\exp(t_0/\tau_i) - 1] \exp(-t/\tau_i)} \qquad (i = 1, 2) . \tag{4}$$

The vortex creep relaxation times which appear in equation (4) are, from equation (I.32),

$$\tau_i = \frac{\omega_{cr}{}^i kT}{|\dot{\Omega}| E_p{}^i} = \left[\frac{kT}{\Omega_c \rho_i \kappa r \xi_i b_i}\right] t_s , \tag{5}$$

where E_p is the energy gain (per nucleus) from the pinning of a vortex line, $\omega_{cr} \equiv (\Omega - \Omega_c)_{cr}$ the critical lag between Ω_c and the superfluid rotation rate Ω for unpinning, ξ is the coherence length of the superfluid, ρ its density, κ the quantum of vorticity, and r the distance from the rotation axis. It is possible that other boundary layers, separating additional regions with distinct τ values, exist in the star; we shall see that one boundary layer, and hence two such internal torques, suffice to fit the data at present.

The third torque, N_A, we identify as coming from the boundary region which separates regions 1 and 2, as shown in Figure 2. Glitches originate in the sudden unpinning of pockets of pinned vorticity in such boundary regions, and these are therefore the regions through which vortices move. We have proposed in Paper I a simple model for the glitch and subsequent changes in the vortex creep in a boundary region, namely that in a given glitch, some N vortices in region G unpin, move through region B, and repin in region G′, as likewise depicted in Figure 2. We found in Paper I that the internal torque N_A, which describes the recoupling of vortex creep in the regions G and G′, initially increases linearly with time, and may be written (cf. eq. [I.56]) during this epoch as

$$N_A \approx \frac{|N|}{I} \frac{I_A t}{t_B} = \dot{\Omega}_\infty{}^2 \left(\frac{I_A}{\delta\Omega_B}\right) t . \tag{6}$$

Here $\delta\Omega_B$ is the sudden decrease in the superfluid rotation rate caused by the outward motion of unpinned vortices through region B at the glitch. It defines a time scale (cf. eq. [I.52])

$$t_B = \frac{\delta\Omega_B}{|\dot{\Omega}_\infty|} = \frac{\delta\Omega_B}{\Omega_c} t_s . \tag{7}$$

In this simple model, there is a fourth internal torque, N_B, associated with the recoupling via vortex creep of region B of Figure 2. We show in the following section that this torque begins to be significant only when the torque N_A goes nonlinear. We note that the last timing fits to the postglitch observations of Downs (1981) extend to 153, 97, 99, and 388 days before the next glitch and cover data chains of about 80–150 days. Downs finds that $\dot{\Omega}_c$ increases linearly with t throughout his entire data base, once the relaxation described by N_1 and N_2 is complete. This then implies that throughout the observations, N_A has not gone

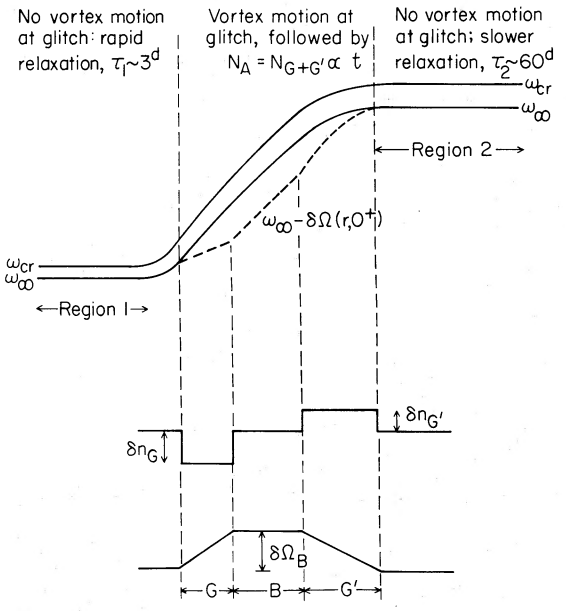

FIG. 2.—A schematic description of the boundary region. The distance from the rotation axis increases to the right, and density to the left. We have marked the regions 1 and 2 associated with the creep relaxation times τ_1 and τ_2 on the figure, as well as the boundary region between them. The upper figure gives the variation of ω_{cr} and ω_∞. The middle figure shows the change in vortex density in the glitch, according to our model of vortex unpinning and repinning in the boundary layer. The lower figure shows the resulting decrease $\delta\Omega(r, 0^+)$ in the superfluid rotation rate; $\Omega \to \Omega - \delta\Omega(r, 0^+)$ in a glitch.

TABLE 2

PARAMETERS OF OUR MODEL OBTAINED BY FITTING EQUATION (9) TO THE OBSERVED $\dot{\Omega}_c$ DATA

Quantity	Glitch 1		Glitch 2		Glitch 3		Glitch 4	
τ_1 (days)	3	4	3	2	3	2	3	6
τ_2 (days)	60	100	60	60	60	60	60	60
Δ (days)	5	5	14	14	5	5	16	22
I_1/I (10^{-2})	0.31	0.33	1.11	1.01	0.19	0.16	1.44	2.37
I_2/I (10^{-2})	0.96	1.57	2.12	2.12	0.54	0.64	2.08	1.85
I_A/It_B (10^{-6}/day)	3.1	2.4	3.7	3.7	6.3	6.3	3.3	3.4

NOTE.—τ_1, I_1/I, and τ_2, I_2/I are the relaxation times and fractional moments of inertia of regions 1 and 2, respectively. I_A/It_B is the slope of the component of $\dot{\Omega}_c(t)$ which increases linearly with t, due to the torque $N_A \equiv N_{G+G'}$ from the glitching regions.

nonlinear and the torque N_B (vortex creep through region B of our model) plays a negligible role; hence we do not include these possibilities in our fits to the postglitch $\dot{\Omega}_c(t)$ data.

We thus attempt to fit to the observational data of Downs with the following expression for $\dot{\Omega}_c(t)$:

$$I_c \ddot{\Omega}_c(t) = N + N_1 + N_2 + N_A , \tag{8}$$

where N is the external torque acting on the star, N_1 and N_2 are the distinct torques specified by equation (4), and N_A is given by equation (6).

In comparing our model with observations, we must also take into account the uncertainty in the actual date of each glitch. The first observation date after each of the first four glitches is some Δ days after the glitch, where $0 \leq \Delta \leq \Delta_m$, Δ_m being the time between the last preglitch observation and the first postglitch observation. In our fits, we derive $\dot{\Omega}_c$ values from the observed $\dot{P}$ values given by Downs, and compare the value of $[\dot{\Omega}_c(t) - \dot{\Omega}_c(0)]_{obs}$ we obtain from the observations ($t = 0$ being the date of the first postglitch data point) with:

$$\dot{\Omega}_c(t + \Delta) - \dot{\Omega}_c(\Delta) = \sum_{i=1}^{2} \frac{|N|}{I_c}\frac{I_i}{I} \cdot \frac{\exp(-\Delta/\tau_i)[\exp(t_0/\tau_i) - 1]}{1 + \exp(-\Delta/\tau_i)[\exp(t_0/\tau_i) - 1]} \frac{1 - \exp(-t/\tau_i)}{1 + \exp[-(t + \Delta)/\tau_i][\exp(t_0/\tau_i) - 1]} + \frac{|N|}{I_c}\frac{I_A}{I}\frac{t}{t_B} . \tag{9}$$

Using equations (4), (5), and (6), the first two terms have the free parameters I_i/I, Δ, and τ_i. The third term has the slope, I_A/It_B (I_A/I cannot be separately fitted). We fit each postglitch data set for $\dot{\Omega}_c(t) - \dot{\Omega}_c(0)$ separately with equation (9), searching numerically for the parameters that yield the least sum of squared differences.

We plot in Figures 1*a*–1*h* the fit $\dot{\Omega}_c(t + \Delta) - \dot{\Omega}_c(\Delta)$, given by equation (9), together with the $\dot{\Omega}_c(t) - \dot{\Omega}_c(0)$ values derived from $\dot{P}$ observations. Table 2 gives the values we have obtained from our fits. The best fits for τ_1, τ_2 are (4^d, 100^d), (2^d, 60^d), (2^d, 60^d), (6^d, 60^d) for the four postglitch fits, respectively. The choice (3^d, 60^d) gives a fit that is close to the best fit in all four cases, in the sense that at each data point the difference between the fit with (3^d, 60^d) and the best fit is less than the root mean square scatter of data points with respect to the best fit. We display both fits in Figure 1. Although we have six parameters altogether, we find it encouraging that independent fits to each postglitch relaxation give similar values for all the parameters involved, and are indeed consistent with the same values for τ_i. *We conclude that the basic elements of the postglitch behavior observed by Downs are contained in the torques, N_1, N_2, and N_A.* In Figure 3 we illustrate the separate contributions of these three torques to $\dot{\Omega}_c(t)$ for our fit of equation (9) to the data following glitch 4. Note that the torques N_1, N_2, and N_A dominate the behavior of $\dot{\Omega}_c(t)$ in distinguishable successive time intervals; the variation in $\dot{\Omega}_c(t)$ in, say, $t \lesssim 25^d$ reflects N_1, that in $25^d \lesssim t \lesssim 150^d$ reflects N_2, and the linear $\dot{\Omega}_c(t)$ at $t \gtrsim 150^d$ reflects N_A. The data following each of the other three glitches also divide naturally into such phases, in each of which the evolution of $\dot{\Omega}_c(t)$ is dominated by one of the torques N_1, N_2, N_A.

We note that the relaxation time τ is expected to vary within each of the regions 1 and 2. A realistic expression for the torques N_1 and N_2 would contain a superposition of torques with different τ_i. For example, N_1 would contain a range of relaxation times of the order of a few days, and possibly shorter relaxation times as well. As can be seen in equation (4) (and is discussed in detail in Paper I), as long as $\tau \ll t_0$, each such torque would cause a sharp "Fermi function" recoupling in $\dot{\Omega}_c(t)$, i.e., a relaxation process lasting some τ days about $t = t_0$. For each of the first four glitches only two or three postglitch data points are available within t_0 days; the average is not complete enough to enable one to resolve a family of such τ's. We therefore described the entire region 1 with a single τ in our fits. Similarly, a single τ was used for region 2.

There are two features in the data distinct from the smooth postglitch relaxation we model by equation (9). These are a small glitch ($\Delta\Omega_c/\Omega_c \sim 10^{-8}$) following glitch 2, represented by a single point in the $\dot{\Omega}_c$ data, and a discontinuity in $\dot{\Omega}_c$, but not in its slope, some 650–750 days after glitch 3 [the last three data points for $\dot{\Omega}_c(t)$ lie on a straight line with the same slope as, but displaced from, the earlier data points already in the linear $\dot{\Omega}_c(t)$ regime]. These will be addressed in future work concerning irregularities and noise in vortex creep. We have not included either of these features in our fits, but the data points are indicated in Figure 1.

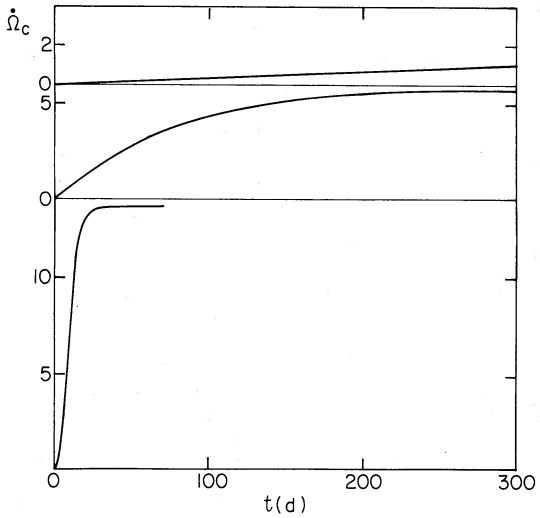

FIG. 3.—The separate effects of the three torques N_1, N_2, and N_A on $\dot{\Omega}_c(t)$. As an example, our model fit (eq. [9]) to postglitch 4 data (shown in Fig. 1*g*) is separated into its components here. We plot $\dot{\Omega}_c(t+\Delta) - \dot{\Omega}_c(t)$ in units of 10^{-13} rad s^{-2} as a function of time in days, as in Fig. 1. The lower curve shows the contribution of N_1; the middle curve, that of N_2; and the upper curve, the contribution of N_A. For about 25 days after the first postglitch timing observations ($t = 0$), the torque N_1 dominates the evolution of $\dot{\Omega}_c$. Following this, the torque N_2 is the dominant internal torque until ~ 150 days. After N_1 and N_2 have settled to their constant steady-state values, N_A is responsible for the persistent linear increase of $\dot{\Omega}_c(t)$ with time. Our fits to $\dot{\Omega}_c$ following the other glitches break down in a similar way into phases in which N_1, N_2, and N_A successively dominate the evolution of $\dot{\Omega}_c$.

III. GLITCH PRECURSORS AND HYSTERESIS

We now examine the glitch-affected boundary region in more detail and take up the related questions of glitch precursors and hysteresis. We first pursue further consequences of the simple model for the postglitch decrease in the superfluid velocity given by equation (I.49) and illustrated in Figure 2. We then consider the more complex structures to be expected if there is appreciable hysteresis, associated with the onset of a glitch before the consequences of the previous glitch have healed.

In our simple model of a glitch (Fig. 2) there are two internal torques associated with a boundary region. The first, N_A, given in equation (6), arises from recoupling of vortices in the regions G and G′ and enables us to determine the combination of model-dependent parameters, I_A/It_B. A second torque, N_B, arises from recoupling of vortices in the region B; here the decrease in superfluid rotation rate following the glitch is assumed to be constant and takes on the maximum value,

$$\delta\Omega(r_B, 0^+) = \delta\Omega_B = \frac{N\kappa}{2\pi r_B^2}, \tag{10}$$

immediately after the glitch; N is the number of vortices which unpin in G. The internal torque associated with region B is given by Equation (I.51):

$$\frac{N_B(t)}{|N|} = \frac{I_B}{I}\frac{1}{1 + [\exp(t_B/\tau_B) - 1]\exp(-t/\tau_B)}, \tag{11}$$

where I_B and τ_B are the inertial moment and average relaxation time of the region, and t_B is given by equation (8). For cases of physical interest $t_B \gg \tau_B$, so that this torque has the characteristic Fermi function behavior, in that it vanishes for $t \ll t_B$, rises to $(I_B/I)|N|$ over a time τ_B about t_B, and remains constant thereafter:

$$\frac{N_B(t)}{|N|} \approx \frac{I_B}{I}\frac{1}{1 + \exp[(t_B - t)/\tau_B]}. \tag{12}$$

If the time between glitches is greater than t_B, and further, if the interval between observations is less than τ_B, such behavior could be resolved in the data, and would enable one to determine I_B, t_B, and τ_B. If the time between glitches, t_g, is of order t_B, it is in principle still possible to infer these quantities from observations close to the time of the next glitch, since these would disclose a departure from the linear behavior of $\dot{\Omega}_c$ immediately prior to the glitch. Finally, if the time between glitches is short compared to t_B, then the next glitch comes along before one has, so to speak, cleared out the consequences of the previous glitch. Consequently, after the next glitch, postglitch behavior will not only reflect what transpired at the time of this new glitch (characterized by some $\Delta\Omega_c$) but also will reflect continuing recovery of those regions affected by the previous glitch which had no time to recouple before the new glitch came along. The three possibilities for $\dot{\Omega}_c$ are illustrated in Figure 4.

At $t \sim t_B$, examination of the more complete expression for N_A given below (cf. eq. [I.54]) shows that departures from linearity will also arise as a consequence of the recoupling of vortices in regions G and G′ (which jointly make up region A):

$$\frac{N_A(t)}{|N|} = \frac{I_A}{I}\frac{1 - (\tau/t_B)\ln[1 + \exp(t_B/\tau - 1)\exp(-t/\tau)]}{1 - \exp(-t/\tau)}. \tag{13}$$

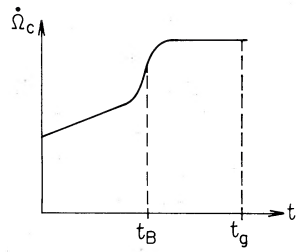

FIG. 4a

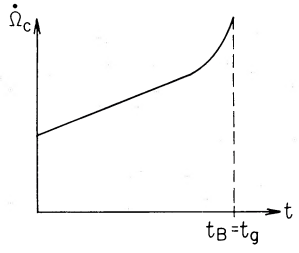

FIG. 4b

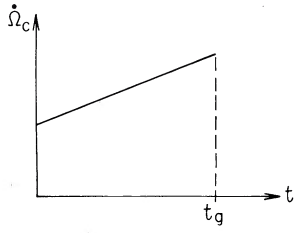

FIG. 4c

FIG. 4.—The effect that the coupling of boundary region B would have on the observed $\dot{\Omega}_c(t)$. The expected signature of $\dot{\Omega}_c(t)$ is shown schematically for three possible cases: *Upper*, if $t_B < t_g$, the time to the next glitch, the region B would completely couple and $\dot{\Omega}_c(t)$ would no longer increase linearly with time. *Middle*, if $t_B \approx t_g$, the nonlinear behavior associated with the coupling of region B signals the imminence of the next glitch, which interrupts it. *Lower*, if $t_B > t_g$, region B is still uncoupled and there is no sign of nonlinearity in $\dot{\Omega}_c(t)$ at the time the next glitch arrives.

These are, however, of order τ_B/t_B compared to the linear variation produced by vortex recoupling in these regions, and hence may be neglected in the limit $\tau_B \ll t_B$.

The postglitch data of Downs enables us to rule out the possibility illustrated in Figure 4*a*: since a constant value of $\dot{\Omega}_c$ is not observed, the simple model does not apply with $t_g \gg t_B$. However, the interesting case, $t_g \approx t_B$, illustrated in Figure 4*b* would seem not inconsistent with the current $\dot{\Omega}_c$ fits of Downs. The last preglitch timing fit involves fitting to data extending over 80–150 days. The departures from linear behavior that would show up in timing fits at $t_g - \tau_B \lesssim t \lesssim t_g$ might not be apparent in these fits, since values of τ_B are expected to lie between 3^d and 60^d if the boundary region connects the regions characterized by these time scales. This possibility is of special interest because, under these circumstances, a glitch would be preceded (over times τ_B) by enhanced vortex creep associated with the lowering of the potential barriers for vortex motion through region B. On this picture, the region B acts as a gradually lowering barrier for vortices unpinned in region G: vortices unpin in G all the time but cannot scatter outward through B unless $\omega(\equiv \Omega - \Omega_c)$ in B is quite close to its steady state value ω_∞. Until vortex creep begins in B, the only way $\delta\omega_B \equiv \omega_B - \omega_\infty$ can change is through the change in Ω_c; thus $\delta\omega_B(t) \approx \delta\Omega_B - |\dot{\Omega}_c|t$ for times t such that $t < t_B - \tau_B$ (cf. eq. [I.41]). When $t \sim t_B - \tau_B(\delta\omega_B \sim |\dot{\Omega}_c|\tau_B)$, vortex creep starts. If outward scattering of unpinned vortices also become feasible at a comparable value of $\delta\omega$, then a local fluctuation leading to vortex unpinning can develop into a glitch since vortex motion through B is now possible. Thus, timing fits within about 60 days preceding a glitch should cast light on whether this scenario is operative. Since one does not know when a glitch will come, the above chain of reasoning points to the desirability of monitoring the Vela pulsar over intervals small compared to 60^d.

The possibility $t_B \gg t_g$, illustrated in Figure 4*c*, if realized in practice leads to considerable hysteresis in $\dot{\Omega}_c(t)$ and $\delta\Omega$. For example, suppose that glitch 3 occurred at a time t_g much less than t_B for glitch 2, and that it had a shape consistent with our simple model, but with parameters I_A, I_B, and $\delta\Omega_B$ which are different from those which characterize glitch 2. The resulting $\delta\Omega$ curve after glitch 3 might then look like Figure 5. As a consequence, at a time $\sim t_B$, after glitch 3, the region B′ (which reflects glitch 2, not glitch 3) will recouple.

Has such recoupling been observed? In the $\dot{\Omega}_c(t)$ observations following glitch 3, there is a jump $\Delta\dot{\Omega}_c/\dot{\Omega}_c \approx 6 \times 10^{-4}$ between the timing observations of Downs at $t = 548$–650 days after his first postglitch observation and those at later times $t > 757$ days (see Fig. 1*e*, *f*). On either side of this apparent jump, $\dot{\Omega}_c(t)$ is linear with little, if any, change in slope across the jump. If the jump was due to the recoupling of a region such as B in our simple model with no hysteresis, $\dot{\Omega}_c$ would be constant after this increase, as shown in Figure 4*a*. The persistence of the linear increase in $\dot{\Omega}_c(t)$ after this event suggests that only one of several such regions, each with a different $\delta\Omega$, recoupled. This kind of partial recoupling is just what one would expect if the $\delta\Omega$ profile after glitch 3 includes effects of hysteresis; for example, the observed recoupling could be associated with a region such as B′ in Figure 5.

Let us pursue this possibility further. Since $\delta\Omega$ is a constant ($\delta\Omega_{B'}$) throughout B′, this recoupling would take place at a time $\sim t_{B'} = \delta\Omega_{B'}/|\dot{\Omega}|_\infty$. Since $t_{B'}$ is bounded by $650^d \lesssim t_{B'} \lesssim 757^d$, $\delta\Omega_{B'}$ is likewise bounded by $7.8 \times 10^{-5} \lesssim \delta\Omega_{B'}/\Omega_c \lesssim 9.1 \times 10^{-5}$. Any discontinuity in the constant slope of $\dot{\Omega}_c(t)$ associated with such an event would then correspond to the subsequent linear recoupling of a region such as G″ in Figure 5 (which would start to recouple at $t = t_{B'}$). The observed event following glitch 3 involved a jump, $\Delta\dot{\Omega}_c/\dot{\Omega}_c = 6 \times 10^{-4}$, which we can identify as $I_{B'}/I$. Any discontinuity in $\ddot{\Omega}_c$ (the observational limits on this are -1.1×10^{-21} rad s^{-2} d$^{-1} \lesssim \Delta\ddot{\Omega}_c \lesssim 4.5 \times 10^{-22}$ rad s^{-2} d^{-1}), would reflect the difference in contributions from regions G″ and G′.

The case $t_B \sim t_g$, the time of the next glitch, is both possible and physically appealing in that there will then be little or no hysteresis and glitches would originate at more or less the same domain in the star. We therefore take the further step of inquiring

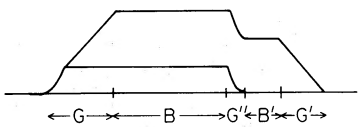

FIG. 5.—A schematic description of possible hysteresis in the glitching regions. At the time, say, glitch 3 occurs, the $\delta\Omega$ caused by the previous glitch, glitch 2, is only partially healed. The lower curve shows this remnant, $\delta\Omega(t_g) \equiv \delta\Omega(0^-) \neq 0$, just before glitch 3. The upper curve shows the resulting $\delta\Omega(0^+)$ after glitch 3. This includes both the remnant from glitch 2 and the $\delta\Omega$ cased by glitch 3.

TABLE 3

PARAMETERS OF OUR SIMPLE MODEL (eq. [10]) FOR THE EFFECT OF THE GLITCH IN THE BOUNDARY REGION

Quantity	Glitch 1	Glitch 2	Glitch 3	Glitch 4
$t_B = t_g$ (days)	900	1485	1000	1170
$\delta\Omega_B \equiv \lvert\dot{\Omega}_\infty\rvert t_B$ (10^{-2} rad s^{-1})	0.76	1.26	0.85	0.99
I_A/I (10^{-2})	0.28	0.55	0.64	0.39
I_B/I (10^{-2})	1.97	0.80	1.33	1.77
$X_0 \equiv I_A/I_B$	0.14	0.69	0.48	0.22

NOTE.—$\delta\Omega_B$ is the glitch induced decrease in superfluid rotation rate in the region B. I_A/I and I_B/I are the fractional moments of inertia of the regions A = G + G′ and B, respectively.

what the glitch parameters I_B and I_A might be under these circumstances for the first four glitches. As we have emphasized, there is no hysteresis in this case; we know $(I_A/2 + I_B)$ and (I_A/It_B), so that the condition $t_B = t_g$ serves to specify not only $\delta\Omega_B$, but also I_A and I_B. It is moreover clear that if $x_0 \equiv I_A/I_B$ for $t_B = t_g$, then for values of $x \equiv I_A/I_B$ less than x_0, $t_B < t_g$, while for $(I_A/I_B) \geq x_0$, $t_B > t_g$. Thus for the first four glitches, there is a definite association between x and t_B (or $\delta\Omega_B$), provided hysteresis effects do not play a significant role.

Our values of I_A, I_B, t_B, $\delta\Omega_B$, and x_0 are given in Table 3. Since, as we have noted, no significant events of the type illustrated in Figure 4*a* have been seen, to the extent that our simple model with no hysteresis is appropriate we conclude that the ratio I_A/I_B must be $\gtrsim x_0$ for the parameters which characterize the first four glitches. Finally, we note that the parameters of Table 3 provide a useful starting point for an examination of glitch-to-glitch correlations, a question we hope to address in a future paper.

In developing our model in Paper I, and applying it to the Vela pulsar in this paper, we have neglected changes in vortex density associated with the glitch and concentrated on the way in which changes in the superfluid and crust rotation rates, $\delta\Omega$ and $\Delta\Omega_c$, influence the vortex creep process. We can now justify this approximation for the Vela pulsar. As may be seen in Figure 2, for a given glitch, the initial (and largest) change in vortex density δn occurs in the unpinning and repinning regions of widths G and G′: it is given by

$$\kappa\delta n_G = -r(\delta\Omega_B/G)\,, \tag{14}$$

$$\kappa\delta n_{G'} = r(\delta\Omega_B/G')\,. \tag{15}$$

These changes in vortex density lead to the changes in superfluid rotation $\delta\Omega$ rate given in Figure 2 for our glitch model. At later times, the perturbations in vortex density tend to heal as vortex creep gradually picks up. Using our results for the Vela pulsar, we find:

$$\kappa\delta n_G \sim \kappa\delta n_{G'} \sim \delta\Omega_B \cdot (I/I_A) \sim 1 \text{ rad s}^{-1}\,. \tag{16}$$

On the other hand, the overall vortex density is

$$\kappa n = 2\Omega + r\frac{\partial\Omega}{\partial r} \approx 2\Omega + r\frac{d\omega_\infty}{dr} > 2\Omega = 140 \text{ rad s}^{-1}\,. \tag{17}$$

for the Vela pulsar. Hence, the results are indeed consistent with taking $\delta n/n \ll 1$ for this pulsar. Note, however, that our model treats vortex unpinning and repinning in regions G and G′ as being uniform; in other words, we have averaged out density fluctuations associated with vortex pockets. A treatment that resolves the effects of individual vortex pockets in the recoupling of the glitch regions to $\dot{\Omega}_c$, or in noise due to unpinning and repinning, might well lead to vortex density fluctuations which are sufficiently localized that the corresponding values of δn become comparable to n. We plan to return to this question in the future.

IV. PINNING PARAMETERS

Encouraged by our success in explaining the postglitch behavior observed by Downs for the first four glitches, we now take up the question of whether by combining theory with observation we can learn something about the nature of the regions of pinned vorticity in the Vela pulsar. In so doing, we lay the groundwork for our examination of what postglitch behavior tells us about the internal temperature of the neutron star.

We have adopted as a working hypothesis that the internal torques, N_1 and N_2, represent the response of distinct regions of pinned vorticity to a glitch. These regions are characterized by relaxation times $\tau_1 \sim 3^d$, $\tau_2 \sim 60^d$. The torque N_A describes the response of the boundary between these regions. Our fit to the observational data leads to inertial moments of these regions, I_1/I, I_2/I, I_A/I which are in the 10^{-2} range. This is the range to be expected for a 1.4 $M_\odot$ neutron star with pinning regions which lie between stellar densities ρ_{13} (ρ in units of 10^{13} g cm^{-3}) such that $3 \lesssim \rho_{13} \lesssim 20$, provided the star obeys a reasonably stiff equation of state (Pandharipande, Pines, and Smith 1976; Pines 1980; Nandkumar 1983). This part of our model is thus consistent with microscopic theory.

From our expression for the relaxation time, equation (5), we see that the only quantity which may be expected to vary sharply between regions 1 and 2 in the sense of reflecting a transition in the physics of pinning is b, the spacing along the vortex line

between effective pinning centers. The other quantities involved, ρ, T, and Δ, all vary continuously through the pinning layers and would not exhibit transitions in their values by a factor of ~ 20 between the regions 1 and 2. Thus in region 2, with its $\sim 60^{\rm d}$ relaxation time scale, each vortex is pinned some 20 times more densely along its length than in region 1. There are, however, three distinct possibilities for these regions:

i) Region 2 ($\tau \sim 60^{\rm d}$) corresponds to "strong" pinning; region 1 ($\tau \sim 3^{\rm d}$) to "weak" pinning.
ii) Region 2 corresponds to strong pinning; region 1 to "superweak" pinning.
iii) Region 2 ($\tau \sim 60^{\rm d}$) corresponds to weak pinning, region 1 to "superweak" pinning.

The nature of the different pinning regimes (strong, weak, superweak) and the criteria for the transitions between them are discussed in the Appendix. As we also discuss there, we expect that the boundary region which separates the distinct pinning regimes will encompass densities $\rho_{13} \sim 8$; in what follows we assume that the transition from one kind of pinning to another will occur in this vicinity. If we had at present accurate microscopic treatments of the energy gap Δ as a function of ρ, and moreover, could calculate with some accuracy the pinning energies, E_p, for each of the possibilities, it would be straightforward to combine theory and observation to determine uniquely the nature of pinning in the regions responsible for the observed $3^{\rm d}$ and $60^{\rm d}$ relaxation times. However, as we discuss in some detail in the Appendix, the current status of microscopic calculations of Δ and E_p is such that any of these three possibilities is consistent with microscopic theory. Still it is illuminating to examine the results of model calculations for the variation of pinning parameters and relaxation times throughout regions 1 and 2 for each of the above possibilities.

For the Vela pulsar, equation (5) may be written as:

$$\tau(\mathrm{d}) = \frac{280 T_7 \Delta(\mathrm{MeV})}{r_6 (k_{\rm F})^4 (b/40)}, \tag{18}$$

where T_7 is the temperature of the inner crust in units of 10^7 K, r_6 the location of the pinning layer in units of 10^6 cm, b is given in fermis, and $k_{\rm F}$, the Fermi wavenumber for the superfluid neutrons, is given in fm^{-1}. We consider first the possibility [cases (i) and (ii)] that the region which is characterized by a vortex creep relaxation time, $\tau_2 \sim 60^{\rm d}$, is one in which vortex lines are strongly pinned to crustal nuclei. The spacing between effective pinning centers along a vortex line is then given by $b \sim b_z$, the internuclear spacing, and equation (18) becomes

$$\tau_2(\mathrm{d}) = \tau^{\rm s}(\mathrm{d}) = \frac{280 T_7 \Delta(\mathrm{MeV})}{(k_{\rm F})^4 (b_z/40) r_6}. \tag{19a}$$

According to Table 4 (cf. the Appendix), the strong pinning region is $3 \lesssim \rho_{13} \lesssim 8$. The calculated variation to be expected for τ_s throughout this region is shown in Figure 6a; there the temperature, T_7, which sets the scale of τ_2, is chosen in such a way that the average over the strong pinning region satisfies

$$\langle \tau_2 \rangle \approx 60^{\rm d} = \langle \tau_2{}^{\rm s}(\mathrm{d}) \rangle = 280 \left\langle \frac{\Delta(\mathrm{MeV})}{(k_{\rm F})^4 (b_z/40) r_6{}^2} \right\rangle_2 T_7 . \tag{19b}$$

If case (i) applies, then the density region, $8 \lesssim \rho_{13} \lesssim 11$, is one of weak pinning, so that in this region $b = b_z{}^3/\xi^2 \pi \gamma_4$ where $\gamma_4 \sim 1$ is a factor which reflects our lack of knowledge of the effective radius of the vortex core for pinning, as discussed in the Appendix. We thus write

$$\tau_1(\mathrm{d}) = \tau^{\rm w}(\mathrm{d}) = 94 \gamma_4 \frac{T_7}{r_6 \Delta(\mathrm{MeV}) (k_{\rm F})^2 (b_z/40)^3} \tag{20a}$$

$$\langle \tau_1 \rangle \approx 3^{\rm d} = \langle \tau_1{}^{\rm w}(\mathrm{d}) \rangle \approx 94 \gamma_4 \left\langle \frac{1}{r_6 \Delta(\mathrm{MeV}) (k_{\rm F})^2 (b_z/40)^3} \right\rangle_1 T_7 . \tag{20b}$$

The calculated variation to be expected for $\tau^{\rm w}$ throughout the latter region is likewise shown in Figure 6*a*.

On the other hand, if case (ii) applies, with superweak pinning throughout the density region, $8 \lesssim \rho_{13} \lesssim 20$, say, since we lack at present any calculations of superweak pinning energies, then the observation of an "average" $3^{\rm d}$ relaxation time simply tells us that $\langle b^{\rm sw} \rangle$, the average effective distance between pinning sites along a given vortex line, is $\sim 20 b_z$. We show superweak pinning qualitatively for the cases (i) and (ii) with the dashed line in Figure 6*a*.

For case (iii), the $60^{\rm d}$ time is to be attributed to a weak coupling region; one thus uses equation (20a), but the average carried out over the density region $3 \lesssim \rho_{13} \lesssim 8$:

$$\langle \tau_2 \rangle \approx 60^{\rm d} = \langle \tau_2{}^{\rm w}(\mathrm{d}) \rangle = 94 \gamma_4 \left\langle \frac{T_7}{r_6 \Delta(\mathrm{MeV}) (k_{\rm F}{}^2) (b_z/40)^3} \right\rangle_2 . \tag{21}$$

The calculated variation in $\tau^{\rm w}$ (with T_7 chosen so as to yield eq. [20b]) is shown in Figure 6*b*; for $\rho_{13} \gtrsim 8$, the superweak pinning region, matters are the same as for case (ii); one knows only that $\langle b^{\rm sw} \rangle \sim 20 \langle b^{\rm w} \rangle$.

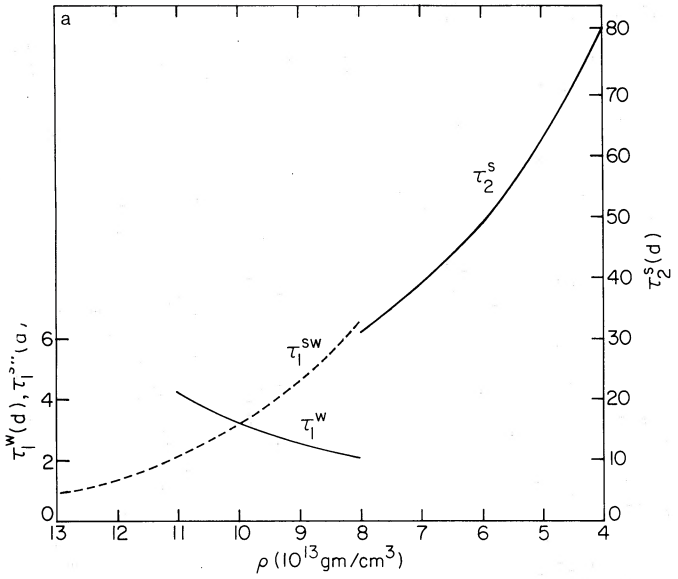

FIG. 6a

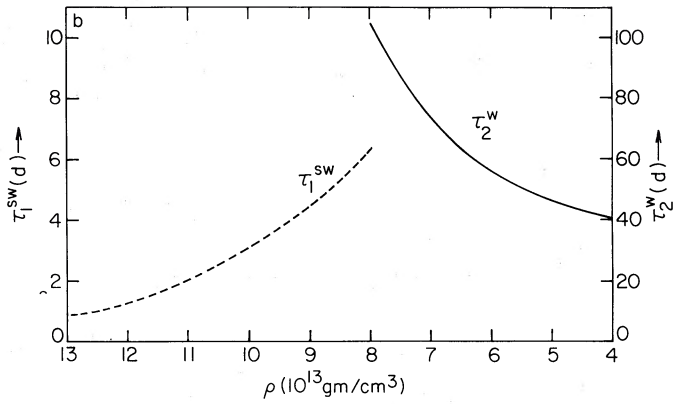

FIG. 6b

FIG. 6.—(*a*) Relaxation times τ_2^s and τ_1^w in the cases (i) and (ii). τ_2^s, corresponding to strong pinning at the lower densities, refers to the axis on the right; τ_1^w calculated for weak pinning of the intermediate densities refers to the left axis. The dashed line shows the relaxation time, τ_1^{sw}, for superweak pinning qualitatively, and also refers to the left axis. Superweak pinning obtains at $\rho \gtrsim 1.1 \times 10^{14}$ g cm^{-3} in case (i) and at $\rho \gtrsim 8 \times 10^{13}$ g cm^{-3} in case (ii). The run of τ_2^s with density is given in eq. (19a) through its dependence on $\Delta(\rho)$, $k_F(\rho)$, $b_z(\rho)$, and is calculated from Table 4. For τ_2^s, we chose $T_7 = 0.07$, such that $\langle \tau_2^s \rangle = \tau_2 \approx 60^d$. τ_1^w is calculated from eq. (20a). $\langle \tau_1^w \rangle = \tau_1 \approx 3^d$ with the average taken over $8 \lesssim \rho_{13} \lesssim 11$ corresponds to $T_7 = 0.03$. (*b*) Relaxation times τ_2^w and τ_1^{sw} in the case (iii). The dashed line for τ_1^{sw} is, again, only qualitative. τ_2^w is given in eq. (20a), with T_7 taken to be 1.5, such that $\tau_2 \approx 60^d = \langle \tau_2^w \rangle$ (eq. [21]).

V. INTERIOR TEMPERATURE

From equations (19) and (21) it is straightforward to obtain estimates of the temperature of the Vela pulsar at the densities which characterize the pinning layers. Given the age of this pulsar ($\gtrsim 10^4$ yr), these layers are part of the isothermal core of the star (Nomoto and Tsuruta 1981; Richardson *et al.* 1982), so the temperature we estimate is actually the central temperature.

If the 60^d relaxation time is attributed to a region of strong pinning, i.e., in either case (i) or case (ii), we find from (19) that

$$T_7^{\text{strong}} = 0.21 r_6 \left\langle \frac{\Delta(\text{MeV})}{k_F^4 (b_z/40)} \right\rangle^{-1} \approx 0.07 , \tag{22}$$

on making use of Table 4 and Figure 6*a*. Further, for strong pinning to characterize this region, we show in the Appendix (eq. [A5]) that there must be a lower bound on Δ; hence there is an upper bound for T_7, which does not depend on a particular gap calculation, but follows from the existence of strong pinning. It is, on making use of equation (A5),

$$T_7^{\text{strong}} \lesssim 0.16 \left(\frac{\gamma_1}{\gamma_2}\right)^{1/2} \left\langle \frac{Z/50}{r_6 k_F^{9/2} (b_z/40)^{5/2} (R_N/7)^{1/2}} \right\rangle^{-1} \approx 0.13 \left(\frac{\gamma_1}{\gamma_2}\right)^{1/2} , \tag{23}$$

where γ_1 and γ_2 reflect uncertainties in our knowledge of the pinning energy and the energy required to pull a nucleus from its equilibrium site, respectively. We expect these quantities to vary through the pinning region. In Table 4 (see the Appendix) we give values of γ_1 for different densities in the pinning region for a particular pinning calculation. Here and in the following we treat γ_1 and γ_2 as constants for simplicity. For given microscopic results these constants can be evaluated as weighted averages defined by equations (22) and (23) and the inequality (A5). In equation (23), we have taken $r_6 = 1$, $R_N = 7$ fm, $Z = 50$.

If on the other hand, the 60^d relaxation time is attributed to a region of weak pinning, we find from (21) that

$$T_7^{\text{weak}} \approx \frac{0.64}{\gamma_4} r_6 \left\langle \frac{1}{\Delta(\text{MeV}) k_F^2 (b_z/40)^3} \right\rangle^{-1} \approx \frac{1.5}{\gamma_4} \tag{24}$$

on using Table 4 and Figure 6*b*. Since strong pinning is not present in this region, we obtain a bound on Δ by inverting the inequality (A5):

$$\Delta \lesssim 1.4 \left(\frac{\gamma_2}{\gamma_1}\right)^{1/2} \left(\frac{Z}{50}\right) \left(\frac{b_z}{40}\right)^{-3/2} (k_F)^{-1/2} \left(\frac{R_N}{7}\right)^{-1/2} . \tag{25}$$

On the other hand, since superweak pinning is also not present in the region, we obtain a lower bound on Δ from equation (A7). On substituting these inequalities for Δ into (21), and calculating the resulting average over values of k_F and b_z, we obtain

$$\frac{0.4}{\gamma_3 \gamma_4} \lesssim T_7^{\text{weak}} \lesssim \frac{0.9}{\gamma_4} \left(\frac{\gamma_2}{\gamma_1}\right)^{1/2} . \tag{26}$$

The γ_i are taken as constants to represent weighted averages. Note, however, that the averaging in the inequality (26) based on equation (21) is different from the averaging in the inequality (23) based on equation (19). The factor γ_3 characterizes our lack of knowledge of the details of the transition to superweak pinning. These bounds again do not depend on a particular gap calculation.

Standard cooling calculations (Tsuruta 1979, 1981; Glen and Sutherland 1980; Nomoto and Tsuruta 1981; Van Riper and Lamb 1981; Richardson *et al.* 1982) predict internal temperatures ~a few $\times 10^7$ to 10^8 K or more for the Vela pulsar. Thus if the 60^d time is associated with weak pinning, our results equations (24) and (26) are marginally consistent with some of the standard cooling scenarios of Glen and Sutherland (1980) and Van Riper and Lamb (1981). However, there are considerable uncertainties in the standard cooling calculations, in particular concerning the effect of strong magnetic fields on opacities in the neutron star crust (Tsuruta 1983). Thus in the case of weak pinning at densities $\lesssim 8 \times 10^{13}$ g cm^{-3} one cannot conclude from our internal temperature estimate that some nonstandard cooling history involving a fast-cooling pion condensate or quark component is called for. On the other hand, if strong pinning is present in this region, the internal temperatures we infer from equations (22) and (23) are clearly too cold for standard cooling, and would require a fast cooling component in Vela.

Observational upper limits to the unpulsed surface X-ray flux from the Vela pulsar (Harnden *et al.* 1979) are consistent with the surface and associated internal temperature range predicted by standard cooling calculations. The surface temperatures we infer from our estimates of the interior temperature using the temperature profiles given by Gudmundsson, Pethick, and Epstein (1982) are well below these upper limits.

An observational means of distinguishing between the options of moderate internal temperatures (weak pinning) and very low internal temperatures (strong pinning) is provided by comparing the energy dissipation expected in either case with detections of, or upper limits on, the surface thermal flux. As we saw in Paper I (eq. [I.57]), the rate of energy dissipation due to vortex creep is proportional to an average value of ω_∞, the steady state lag between the pinned superfluid and crust rotation rates:

$$\dot{E}_{\rm diss} \approx |\dot{\Omega}| \int dI_p \omega_\infty \approx |\dot{\Omega}| I_p \bar{\omega}_{\rm cr} \tag{27}$$

on noting that $\omega_\infty \simeq \omega_{\rm cr}$ and introducing an average value $\bar{\omega}_{\rm cr}$ of $\omega_{\rm cr}$, the critical lag for unpinning, which from equation (I.11) is

$$\omega_{\rm cr} = \frac{E_p}{\rho \kappa r b \xi} . \tag{28}$$

Constraints imposed on $\dot{E}_{\rm diss}$ by a detection or upper limit of the surface X-ray flux will give information on $\bar{\omega}_{\rm cr}$ through equation (27). Table 5 of the Appendix gives $\omega_{\rm cr}$ as a function of density in the pinning layers for both strong and weak pinning, based on the specific model used to calculate Table 4. Depending on whether or not one has appreciable regions of strong pinning present ($I_2^s/I \sim 10^{-2}$), the resulting values of $\bar{\omega}_{\rm cr}$ differ by a factor ~35. Thus, one expects $\bar{\omega}_{\rm cr} \sim 7$ rad s^{-1} in the case of strong pinning in the region $\rho_{13} \lesssim 8$, and $\bar{\omega}_{\rm cr} \sim 0.2$ in the case of weak pinning in this region. These averages are taken over the entire pinning region, and hence are less than half the average values for $\rho_{13} \lesssim 8$, as the values of $\omega_{\rm cr}$ at the higher densities are negligible in comparison. The upper limit to the unpulsed X-ray flux from Vela, $L_x \lesssim 10^{33}$ ergs s^{-1} (Harnden *et al.* 1979) gives $\bar{\omega}_{\rm cr} \lesssim 1$ rad s^{-1}, and hence favors weak pinning. Detected X-ray fluxes (Helfand 1982) from two radio pulsars PSR 1929+10 (detected as a point source) and PSR 0950+08 likewise yield interesting upper limits on $\bar{\omega}_{\rm cr}$. If $I_p \approx 10^{-2}\, I$ is taken to be 10^{43} g-cm^2, these pulsars have $\bar{\omega}_{\rm cr} \lesssim 5.6 \times 10^{-2}$ and $\bar{\omega}_{\rm cr} \lesssim 0.75$, respectively, so that to the extent that the current distance estimates to these pulsars are reliable, we conclude in these cases as well that no significant regions of strong pinning exist.

The instrumental lower limit for soft X-ray detections with the *Einstein Observatory* was $f_{\rm min} \approx 10^{-13}$ ergs cm^{-2} s^{-1} (Helfand 1982). Future X-ray detectors with an improved sensitivity will be able to search for pulsars radiating surface flux associated with energy dissipation by creep, equation (27), out to a larger distance. The limiting distance within which a pulsar with given $\dot{\Omega}$, I_p, and $\bar{\omega}_{\rm cr}$ would be detected with a detector which is sensitive to a soft X-ray flux greater than f is:

$$D = \left(\frac{I_p \bar{\omega}_{\rm cr} |\dot{\Omega}|}{4\pi f} \right)^{1/2} . \tag{29}$$

Normalizing to typical values $I_p = 10^{-2}\, I = 10^{43}$ g-cm^2, $|\dot{\Omega}| = 10^{-14}$ rad s^{-2}, and $f_{\rm E} \approx 10^{-13}$ ergs cm^{-2} s^{-1}, the flux threshold of the *Einstein Observatory*, we find this limiting distance to be

$$D \approx 100 \left(\frac{I_{p,43} |\dot{\Omega}|_{-14} \bar{\omega}_{\rm cr}}{(f/f_{\rm E})} \right)^{1/2} \text{pc} . \tag{30}$$

A future instrument with $f = 0.1 f_{\rm E}$ would push this limit to 300 pc for these representative values. Such a detector might also uncover a new class of hitherto unobserved neutron stars: those with low magnetic fields and/or rotational periods which do not lead to a detectable radio luminosity, but which nonetheless are slowed down by electromagnetic torques. These might be descendents of pulsars whose magnetic fields have decayed or whose rotation rates decreased below the threshold values of $B\Omega^2$ for pulsar activity, but which nevertheless still produce long-wavelength dipole radiation and hence a large enough spin-down rate $\dot{\Omega}$. We further note that if there are neutron stars whose rotation rates at formation are too low to produce pulsar activity, but which nevertheless decelerate by electromagnetic torques, for large enough $\bar{\omega}_{\rm cr}$ and $\dot{\Omega}$ these might be detected through the energy dissipation rate given in equation (27).

VI. CONCLUDING REMARKS

Our principal conclusions are fourfold:

i) The observed complex postglitch behavior of the Vela pulsar after the four glitches which took place during the decade 1969–1979 can be explained as resulting from the coupling of the crust to that part of the neutron superfluid in which vortex lines are pinned to the crustal nuclei.

ii) At least two distinct pinning regions separated by a boundary exist in this pulsar; their inertial moments are $\sim 10^{-2} I$, a result consistent with microscopic theory for neutron matter equations of state which are moderately stiff to stiff. This indicates that the entire star, except for the pinned superfluid, must be included in the "crust" moment of inertia, in agreement with recent calculations which show that the superfluid core of the star couples to the crust on time scales of seconds (Alpar, Langer, and Sauls (1984).

iii) State-of-the-art microscopic calculations do not enable one to decide between the alternatives of strong and weak pinning for the density region $3 \lesssim \rho_{13} \lesssim 8$; however, combining our theoretical results on energy dissipated by vortex creep with X-ray observations of the Vela pulsar and two other pulsars, we conclude that there are no significant regions of strong pinning in these stars. Hence the two distinct pinning regions must correspond to weak pinning and superweak pinning, respectively.

iv) Consequently, the internal temperature of the Vela pulsar is $(1.5 \pm 1) \times 10^7$ K. The quoted errors do not refer to a particular calculation, but rather reflect estimates of the degree of uncertainty introduced by our lack of knowledge of various pinning parameters. This temperature range is consistent with standard cooling scenarios for this pulsar.

In our fit to the timing data we have made the simplest possible assumptions regarding the regions in which vortex creep takes place. For example, we have approximated the expected variation in the distances b between pinning sites for either weak or strong pinning regions by some average values. In practice, we expect a distribution of b-values in either case, a distribution which may in principle be observed as a distribution of those relaxation times which characterize the return of vortex creep in these regions to its steady-state values. These averages will, in fact, differ from one glitch to the next, since the regions through which no vortices travel may be expected to vary from one glitch to the next. Moreover, we have used a highly simplified model for the boundary region. Again, structure in the timing data may arise from pockets of pinned vorticity which are to be expected in this region. Needless to say, it is highly gratifying that none of these expected inhomogeneities are present to such an extent as to preclude agreement at an elementary level between theory and observation.

It will be of great interest to see whether the theory developed here and in Paper I can explain the timing behavior of the Vela pulsar following its fifth and sixth glitches with no significant changes in the average relaxation times τ_1 and τ_2. The recently published timing results after glitch 5 are encouraging in that they seem to have characteristic features which are similar to those observed after the first four glitches. The fit to timing data following this glitch presented by McCulloch *et al.* (1983) consists of a fast exponential relaxation time of 1.6 days, followed by a slower exponential relaxation, with time constant $\tau = 233^{\rm d}$ fitted to a data span of ~ 6 weeks. We expect that the timing data can be fitted equally well, and easily interpreted in physical terms, if one fits $\dot{\Omega}_c(t)$ with the internal torques of our vortex creep model, viz., the torques N_1 and N_2 with time scales $\tau_1 \sim 3^{\rm d}$, $\tau_2 \sim 60^{\rm d}$, and a boundary layer response $N_{\rm A}$ which contributes a term linear in t to $\dot{\Omega}_c$. Such fits to the timing data following glitch 5 will be particularly interesting, as the occurrence time of this glitch is known with an uncertainty of only 18 hr. We also expect $\dot{\Omega}_c(t)$ following glitch 6 (Hamilton, McCulloch, and Royle 1982) to display similar features. Moreover, the study of glitch-to-glitch correlations in our derived quantities I_1, I_2, and $I_{\rm A}$, as well as in "best-fit" values of τ_1 and τ_2, should provide considerable insight into the origin and frequency of giant glitches.

The twin possibilities of glitch precursors and/or hysteresis also deserve further study. It is tempting to conclude from the fact that McCulloch *et al.* find, just before glitch 5, an $\ddot{\Omega}_c$ term which is $2.1 \pm 0.3 \times 10^{-16}$ rad s^{-2} d^{-1}, and hence is lower than the value $3.7 \pm 0.7 \times 10^{-16}$ rad s^{-2} d^{-1} found by Downs in his postglitch 4 data, that a significant part of the boundary layer region relevant to glitch 4 relaxed just prior to glitch 5, a possibility which deserves careful examination.

Improved theoretical calculations of the superfluid energy gap, the pinning energy, and the distance between pinning sites under weak pinning conditions will make possible an improved determination of the pulsar temperature. Microscopic calculations of pinning parameters in the superweak regime are also highly desirable; these will be especially helpful in sorting out the nature and extent of the transition from weak to superweak pinning to the star, as well as providing a basis for an independent estimate of the internal stellar temperature.

Finally we note that the general theory of vortex creep developed in Paper I and applied here to the Vela pulsar with encouraging results offers other astrophysical applications. One particular application is to noise associated with small discrete unpinning events and the response of vortex creep to these. Another interesting application is to many X-ray sources where an accreting neutron star may be subject to variations in the external (accretion) torque on time scales comparable to the relaxation times of vortex creep, so that the response of vortex creep will produce time-varying internal torques. Observationally, the energy dissipation associated with vortex creep may provide a future means of detecting neutron stars which experience an external torque but are not active as pulsars. These further applications of our vortex creep theory will be explored in future work.

We thank G. Downs, D. Helfand, R. Nandkumar, M. Ruderman, and S. Tsuruta for useful conservations. M. A. A. and J. S. thank M. Ruderman, the Columbia Astrophysics Laboratory, and the Departments of Physics and Astronomy, Columbia University for their hospitality. We want to give our special thanks to the Aspen Center for Physics, where our collaborative efforts on this problem began in the summer of 1975, and where they have continued to flourish in subsequent summers.

APPENDIX

In this Appendix we examine predictions of microscopic theory for the various pinning regions. We make the theoretical uncertainties explicit by including uncertainty factors γ_i in several key equations that distinguish the different pinning regimes.

We first examine the pinning energy. The volume pinning effect we have considered in previous work (Alpar 1977; Anderson *et al.* 1982) gives the pinning energy of equation (I.7) and Figure I.2,

$$E_p = \frac{3}{8}\left[\left(\frac{\Delta^2}{E_F}\frac{k_F^2}{3\pi^2}\right)_{out} - \left(\frac{\Delta^2}{E_F}\frac{k_F^3}{3\pi^2}\right)_{in}\right]V . \tag{A1}$$

The quantity in the square brackets is the energy cost per unit volume to create a vortex line core, which is normal matter. The subscripts "out" and "in" refer to values of Δ, k_F, and E_F for the superfluid neutrons outside nuclei and inside nuclei, respectively; V is the geometrical overlap volume of the pinned vortex line (treated as a cylinder of radius ξ) and the nucleus (a sphere of radius R_N):

$$\begin{aligned} V &= \frac{4\pi}{3}R_N^3\left[1-\left(1-\frac{\xi^2}{R_N^2}\right)^{3/2}\right] \quad (\xi < R_N) , \\ V &= \frac{4\pi}{3}R_N^3 \qquad\qquad\qquad\qquad (\xi > R_N) . \end{aligned} \tag{A2}$$

$\xi = 2E_F/\pi k_F \Delta$ is the coherence length of the neutron superfluid. There are two sources of uncertainty in equation (A1). First, the comparison of condensation energies per unit volume between the superfluid inside and the superfluid outside the nuclei, represented by the square brackets in equation (A1), is not exact; it rests on the approximation of separately defined local densities of superfluid neutrons inside and outside the nuclei. Second, the effective volume within which the microscopic structure of the superfluid is changed by pinning may differ to some extent from the geometrical overlap, equation (A2). For example, Thuneberg, Kurkijärvi, and Rainer (1982) have recently carried out a microscopic calculation of the binding of a magnetic vortex to a pinning center of radius R_N in a type II superconductor; they find that quasi-particle scattering by the center leads, in the case $\xi \gg R_N$, to an increase in the pinning volume by a factor $\sim(\xi/R_N)$.

In the following discussion, we shall deal with these uncertainties by taking the pinning energy to be:

$$E_p = \frac{3}{8}\gamma_1\left(\frac{\Delta^2}{E_F}\frac{k_F^3}{3\pi^2}\right)_{out} 2\pi\xi^2 R_N \tag{A3}$$

to scale the dependence of E_p on the gap and density in a simple way. In equation (A3), energy cost per unit volume to create a vortex core is scaled to the value of the condensation energy in the bulk of the superfluid outside the nuclei, while V is taken to be $2\pi\xi^2 R_N$, the approximate geometrical overlap volume as long as $\xi \lesssim R_N$ (which is roughly the case for $\rho \lesssim 7 \times 10^{13}$ g cm^{-3}). The quantity γ_1 takes into account the uncertainty implied in this procedure as well as the uncertainty in the condensation energy. A given model calculation of E_p can then be parameterized by the value of γ_1 it yields. For example, the pinning energy calculated using equations (A1) and (A2) is given in Table 4 (see also Fig. 2 of Paper I). One finds $E_p > 0$ (i.e., pinning occurs) at $\rho \gtrsim 3 \times 10^{13}$ g cm^{-3}; the values of γ_1 tabulated there are obtained by comparing equation (A3) with equations (A1) and (A2).

Strong pinning obtains when the pinning energy is large enough to displace nuclei from their equilibrium sites by an amount sufficient to enable the vortex line to pass through every lattice site on its path, so that the distance between pinning sites along the vortex line is $b \sim b_z$, the internucleon spacing (Anderson *et al.* 1982). To achieve this, one requires $E_p \gtrsim E_L$, the energy to displace

TABLE 4

PINNING PARAMETERS AS A FUNCTION OF DENSITY (in 10^{13} g cm^{-3})

ρ	b_z (fm)	Z	k_f (fm^{-1})	Δ(MeV)	ξ(fm)	E_p(MeV)	E_L(MeV)/γ_2	γ_1
3.41	49	50	0.82	2.8	3.8	0.86	0.46	0.34
4.....	47	50	0.86	2.8	4.0	1.3	0.58	0.44
5.....	43	50	0.93	2.7	4.5	2.0	0.92	0.53
6.....	40	50	1.0	2.5	5.2	2.6	1.6	0.57
7.....	36	50	1.0	2.2	6.1	3.0	2.9	0.57
8.....	33	40	1.1	1.9	7.4	2.8	3.6	0.47
9.....	31	40	1.1	1.7	9.0	2.3	6.0	0.34
10.....	30	40	1.2	1.4	11.0	1.8	10.0	0.24
11.....	28	40	1.2	1.2	14.0	1.3	19.0	0.16
12.....	27	40	1.3	0.85	19.0	0.71	44.0	0.08
13.17	25	32	1.3	0.65	26.0	0.45	96.0	0.04

NOTE.—The values of b_z and Z are interpolated between values given by Negele and Vautherin (1973) at $\rho_{13} = 3.41, 7.93, 13.17$. We stop at $\rho_{13} = 13.17$ as this is the highest density at which parameters of the lattice are given by these authors. The values of Δ are taken from Hoffberg *et al.* (1970). Values of k_F, Δ, and ξ correspond to the density of superfluid neutrons outside the nuclei. E_p is calculated from eqs. (A1–2), E_L from eq. (A4), γ_1 by comparing the calculated values of E_p with eq. (A3).

a nucleus a distance ξ. (If there is a region of strong pinning, it is characterized by $\xi \lesssim R_N$, the radius of a nuclear cluster.) The energy for displacing nuclei by a distance ξ in the lattice can be written as:

$$E_L = \frac{Z^2 e^2}{b_z^3} \xi^2 \gamma_2 , \tag{A4}$$

where the factor $\gamma_2 \sim 1$ allows for our lack of knowledge of the mean displacement of a nucleus to achieve pinning. Depending on the orientation of the vortex lines with respect to the lattice and the actual microscopic mechanism of pinning, the relevant mean displacement in equation (A4) may be somewhat greater or less than ξ. For the specific example tabulated in Table 4 we find that if $\gamma_2 \sim 1$, strong pinning exists for densities, $3 \lesssim \rho_{13} \lesssim 8$, where ρ_{13} is the density in units of 10^{13} g cm^{-3}.

Inspection of Table 4 shows that if the ratio γ_1/γ_2 were a factor of 2 smaller for $3 \lesssim \rho_{13} \lesssim 8$ (as might result, for example, from an overestimate by a factor of 2 of the difference in condensation energy per unit volume for superfluid neutrons inside and outside nuclei, or with $\gamma_2 \sim 2$), there would be no region of strong pinning. It is either of these possibilities which is likely the primary source of uncertainty in the nature of the pinning here; at the densities involved ($\rho \lesssim \rho_0/4$, where ρ_0 is the density of nuclear matter), the low density approximation inherent in the Hoffberg *et al.* (1970) or Takatsuka (1972) calculations of Δ is likely valid. Using (A2) and (A4), it is straightforward to obtain the following criterion for strong pinning:

$$\Delta(\mathrm{MeV}) \gtrsim 1.4(\gamma_2/\gamma_1)^{1/2}(Z/50)(b_z/40)^{-3/2} k_F^{-1/2} (R_N/7)^{-1/2} , \tag{A5}$$

where b_z is in fm and k_F in fm^{-1}.

Weak pinning obtains when $E_p \lesssim E_L$, and the coherence length $\xi \lesssim b_z/2$ (see below). Inspection of Table 4 shows that for this model calculation weak pinning is to be expected for $8 \lesssim \rho_3 \lesssim 11$. However, over this density region existing gap calculations are not as reliable as at lower densities; if the true value of Δ is a factor ~ 2 larger than those calculated in the low-density limit for $10 \lesssim \rho_{13} \lesssim 20$, one would find weak pinning for $8 \lesssim \rho_{13} \lesssim 20$; conversely, if the true value of Δ were some 80% smaller for $\rho_{13} \sim 9$, superweak pinning would begin in this density range. Where weak pinning exists, vortex lines cannot displace nuclei to achieve optimal pinning at intervals $b \sim b_z$. Nor can they bend to pin, as the tension on vortex lines is $E_F k_F \approx 30$–40 MeV/fm. They therefore pin only to those nuclei that coincide with the vortex core. If the effective cross section area of the vortex core for such "geometrical" pinning is $\gamma_4 \pi \xi^2$, with $\gamma_4 \sim 1$, the distance between successive pinning nuclei along the vortex line (the length of vortex core in which there is a single pinning nucleus) is given by:

$$b = \frac{b_z^3}{\gamma_4 \pi \xi^2} , \tag{A6}$$

where b_z^3 represents the volume per nucleus in the lattice. In Table 5 we give calculated values of b, the distance between pinning centers, and $\omega_{cr} \equiv \Omega - \Omega_c$, the critical lag for unpinning, given by equation (28), for two different models. The first is the example of Table 4, in which one has strong pinning for $3 \lesssim \rho_{13} \lesssim 8$, weak pinning for $8 \lesssim \rho_{13} \lesssim 11$; this corresponds to case (i) discussed in the text. The second is the possibility cited above, that $(\gamma_1/\gamma_2) \lesssim 0.2$ for $3 \lesssim \rho_{13} \lesssim 8$, in which case one has weak pinning throughout this density range; it will correspond then to case (iii) considered in the text. The results presented in Table 5 illustrate the dramatic change in b and ω_{cr} which occur with a transition from strong to weak pinning; we see also that for the same density region, these parameters differ substantially, depending on whether or not strong pinning conditions are met.

Superweak pinning obtains when the coherence length $\xi \gtrsim b_z/2$. As illustrated in Figure 1 of Paper I, the vortex line core then encompasses many nuclei within its diameter, so that moving the vortex line makes little difference in the available pinning energy.

TABLE 5

PINNING PARAMETERS AS A FUNCTION OF DENSITY FOR TWO DIFFERENT MODELS OF PINNING ENERGIES AND SUPERFLUID ENERGY GAPS

	Case (i)			Case (iii)		
ρ_{13}	E_p(MeV)	b(fm)	ω_{cr}(rad s^{-1})	E_p(MeV)	b(fm)	ω_{cr}(rad s^{-1})
3.41	0.86	49	12	0.43	2500	0.12
4	1.3	47	15	0.65	2000	0.18
5	2.0	43	18	1.0	1200	0.31
6	2.6	40	18	1.3	700	0.49
7	3.0	36	17	1.5	400	0.76
8	2.8	33	13	1.4	200	1.03
10	1.8	72	2			
11	1.3	39	1.9			

NOTE.—The first model is based on the calculations presented in Table 4 and corresponds to case (i) of the text; the second assumes that E_p is everywhere reduced by a factor of 2 and leads to case (iii) of the text. Our model calculation stops at the transition to superweak pinning.

We take into account our lack of knowledge of just where the transition from strong or weak to superweak pinning occurs, by writing the condition for a transition to superweak pinning as

$$\xi = \frac{2E_F}{\pi k_F \Delta} = \gamma_3 \frac{b_z}{2}. \tag{A7}$$

where $\gamma_3 \sim 1$. Hence where

$$\Delta(\text{MeV}) \gtrsim (0.7/\gamma_3) k_F/(b_z/40)\,, \tag{A8}$$

there will be no regions of superweak pinning present. Here b_z is in fm and k_F in fm^{-1}.

Microscopic calculations do not exist for b and ω_{cr} under superweak pinning conditions. The pinning energy, E_p, is comparable to those which are tabulated in Table 5; however, because $\xi \gtrsim b_z/2$, a given vortex core can pin to many adjacent nuclei simultaneously, what is then relevant is the potential barrier for motion of this configuration from one set of nuclear sites to another. This motion can be described by the same vortex creep equations as those used to treat strong or weak pinners; b is, however, to be interpreted as the distance along the vortex line between the sets of nuclei which constitute an effective pinning site. Clearly b in the superweak regime is considerably greater than the pinning length in the weak pinning regime, while the effective pinning energy *per nucleus*, E_p^{eff}, will be considerably less than the previous energy per nucleus, E_p, of the weak pinning regime. Similarly we expect that representative values of ω_{cr} in the superweak regime will be considerably less than those encountered in the weak pinning regime.

We conclude that either a strong-to-weak or a strong-to-superweak transition at $\rho_{13} \sim 8$ is consistent with current microscopic calculations, as is the possibility of a weak-to-superweak transition at about this density.

REFERENCES

Alpar, M. A. 1977, *Ap. J.*, **213**, 527.
Alpar, M. A., Anderson, P. W., Pines, D., and Shaham, J. 1981, *Ap. J. (Letters)*, **249**, L33.
———. 1984, *Ap. J.*, **276**, 325 (Paper I).
Alpar, M. A., Langer, S., and Sauls, J. A. 1984, *Ap. J.*, submitted.
Anderson, P. W., Alpar, M. A., Pines, D., and Shaham, J. 1982, *Phil. Mag. A*, **45**, 227.
Downs, G. S. 1981, *Ap. J.*, **249**, 687.
Downs, G. S., Manchester, R. N., and Newton, L. M. 1978, *IAU Circ.*, No. 3274.
Glen, G., and Sutherland, P. 1980, *Ap. J.*, **239**, 671.
Gudmundsson, E. H., Pethick, C. J., and Epstein, R. I. 1982, *Ap. J. (Letters)*, **259**, L19.
Hamilton, P. A., McCulloch, P. M., and Royle, G. W. R. 1982, *IAU Circ.*, No. 3729.
Harnden, F. R., Jr., Hertz, P., Gorenstein, P., Grindlay, J., Schreier, E., and Seward, F. D. 1979, *Bull. AAS*, **11**, 424.
Helfand, D. 1982, in *IAU Symposium 101, Supernova Remnants and Their X-Ray Emission*, ed. P. Gorenstein and J. Danziger, (Dordrecht: Reidel).
Hoffberg, M., Glassgold, A. E., Richardson, R. W., and Ruderman, M. 1970, *Phys. Rev. Letters*, **24**, 775.
Manchester, R. N., Goss, W. M., and Hamilton, P. A. 1976, *Nature*, **259**, 291.
McCulloch, P. M., Hamilton, P. A., and Royle, G. W. R. 1981, *IAU Circ.*, No. 3644.
McCulloch, P. M., Hamilton, P. A., Royle, G. W. R., and Manchester, R. N. 1983, *Nature*, **302**, 319.
Nandkumar, R. 1983, private communication.
Negele, J. W., and Vautherin, D. 1973, *Nucl. Phys. A*, **207**, 298.
Nomoto, K., and Tsuruta, S. 1981, *Ap. J. (Letters)*, **250**, L19.
Pandharipande, V. R., Pines, D., and Smith, R. A. 1976, *Ap. J.*, **208**, 550.
Pines, D. 1980, *J. de Phys.*, **C2**, 111.
Radhakrishnan, V., and Manchester, R. N. 1969, *Nature*, **222**, 228.
Reichley, P. E., and Downs, G. S. 1969, *Nature*, **222**, 229.
———. 1971, *Nature Phys. Sci.*, **234**, 48.
Richardson, M. B., Van Horn, H. M., Ratcliff, K. F., and Malone, R. C. 1982, *Ap. J.*, **255**, 624.
Takatsuka, T. 1972, *Progr. Theor. Phys.*, **48**, 1517.
Thuneberg, E. V., Kurkijärvi, J., and Rainer, D. 1982, *Phys. Rev. Letters*, **48**, 1853.
Tsuruta, S. 1979, *Phys. Rept.*, **56**, 237.
———. 1981, in *IAU Symposium 95*, "*Pulsars*," ed. R. Wielebinski and W. Sieber (Dordrecht: Reidel), p. 331.
———. 1983, private communication.
Van Riper, K. A., and Lamb, D. Q. 1981, *Ap. J. (Letters)*, **244**, L13.

M. A. Alpar and D. Pines: Physics Department, University of Illinois, Urbana, IL 61801-3000

P. W. Anderson: Bell Laboratories, 600 Mountain Avenue, Murray Hill, NJ 07974

J. Shaham: Racah Institute of Physics, Hebrew University, Jerusalem, Israel